AIAA-2002-1720

43rd AIAA/ASME/ASCE/AHS/ASC Structures, Structural Dynamics, and Materials Con
22-25 April 2002, Denver, Colorado

AIAA 2002-1720

Roll Maneuver Control of UCAV Wing Using Anisotropic Piezoelectric Actuators

Debashis Sahoo* and **Carlos E. S. Cesnik†**
Department of Aeronautics and Astronautics
Massachusetts Institute of Technology, Cambridge, Massachusetts

ABSTRACT

Aeroelastic control of combat aircraft has been implemented by the static method of aeroelastic tailoring and the active method of discrete control surfaces. With the ongoing development of high authority piezocomposite-based anisotropic actuators, it may be possible to use active wing warping for aeroelastic control, in particular for roll maneuver of the next generation Uninhabited Combat Aerial Vehicles (UCAVs). A preliminary study done on a generic combat aircraft embedded with active fiber composites (AFCs) in the wing skin indicates that an actuator of higher authority than that of presently available AFC is needed to achieve the desired roll rate level. Currently pursued single crystal fiber composite (SCFC) may be the enabler of such technology.

A numerical design environment was developed to design a UCAV in which roll maneuver control can be done using wing warping. This framework includes the novel concept of integrally distributed anisotropic piezocomposite actuators in a composite wing. A test study based on a simple cantilevered plate in the presence of airflow indicated the viability of the framework. An optimization study was then conducted on a UCAV model using a particular passive and active material layup and wing airfoil. The thickness of the aircraft skin was varied and minimum weight configuration found. The study showed that it is possible to achieve the desired roll rate level using SCFC-based wing deformation. The study may be further refined by using different material layups, airfoils, and fuselage shapes. Suitable control loop may also be incorporated in order to guarantee the performance of the vehicle.

INTRODUCTION

Although aeroelastic problems were present since the first human powered flight, they grew into prominence during World War II with the advent of modern high-speed fighter aircraft. Since then, extensive studies have been conducted on aeroelastic control with the objectives of delaying the onset of instabilities, vibration suppression, maneuver control and performance enhancement.

Aeroelastic Tailoring for Performance Enhancement

Aeroelastic performance enhancement may be achieved through the passive technique of aeroelastic tailoring, or several active control techniques, both of which attempt to change the airfoil characteristics (such as angle of attack). Aeroelastic tailoring may be defined as the employment of directional stiffness into aircraft structural design to achieve given performance objectives [1]. One of the earliest works in this field was by Munk [2] in 1949, when he designed a wooden propeller with a fixed pitch. The blades would twist elastically and favorably as the thrust changes. This was accomplished by suitably orienting the grains of the wood.

Development of filamentary composite materials provided a new impetus to aeroelastic tailoring research. In 1969, Waddoups, McCullers and Naberhaus [3] showed that the directional properties of composites could be used to create a coupling between bending and twist deformation. This coupling produced the desired shape control for a supercritical wing they were designing. In the same year, a computer program known as Wing Aeroelastic Synthesis Procedure, also called TSO, was developed by McCullers, Waddoups, et al. [4]. This code was used by Price [5] in the design of the remotely pilotable HiMAT aircraft. Another application of the code was on the X-29 forward swept wing demonstration aircraft [6].

During the 70's and 80's, tailoring was used in the problems associated with stability (divergence and flutter), lateral control effectiveness, and load redistribution [7, 8, 9, 10, 11]. An interesting aspect of aeroelastic analysis and design conducted during the 90's was in replacing the composite wing structural model from a simple laminated plate to an equivalent beam. Such techniques were used for analyzing high aspect ratio composite wings [12, 13, 14, 15].

Aeroelastic tailoring, in isolation, is essentially static in nature and its effectiveness is limited to a design point. Hence, active techniques for aeroelastic performance enhancement started being considered in the mid-70's. There are two basic ways of implementing ac-

*Graduated Research Assistant. Student Member AIAA.

†Associate Professor of Aeronautics and Astronautics. Associate Fellow AIAA, Member AHS. Currently, Associate Professor of Aerospace Engineering, The University of Michigan, Ann Arbor, Michigan.

Copyright © 2002 by the authors. Published by the American Institute of Aeronautics and Astronautics, Inc., with permission.

Copyright © 2002 by the author(s). Published by the American Institute of Aeronautics and Astronautics, Inc., with permission.

tive control technology (see Figure 1). One is through the use of discrete control surfaces such as leading edge and trailing edge flaps. The other is the concept of "deformable airfoil" in which the control surface is seamlessly integrated into the wing structure.

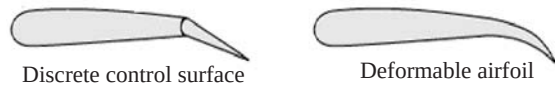

Figure 1: Two different control implementation concepts in lifting surfaces.

Discrete Control Surface Actuation Method for Aeroelastic Control

In 1975, Sandford, Abel, and Gray [16] presented flutter suppression studies on a cantilevered delta wing in the Langley Transonic Dynamics Tunnel. The wing had leading and trailing edge flaps and different active control methods were applied for increasing flutter dynamic pressure. In the early 80s, most of the flutter suppression systems were demonstrated by using wing/stores to induce flutter and control it by special outboard ailerons and flaperons [17].

In 1990, Perry, Mukhopadhayay, Hoadley, and coworkers [18] proposed an Active Flexible Wing (AFW) experiment. It is an aeroelastically-scaled wind tunnel model with highly flexible bend-twist coupled wings. The wings have leading and trailing edge flaps with rotary actuators. Both aeroelastic tailoring and active control techniques were used for flutter suppression. Lazarus, Crawley, and Lin [19] studied aeroelastic control using control surfaces and strain actuation (discussed later) techniques. They did a typical section analysis for the problem and compared both ways of aeroelastic control. More recently, Weisshaar, Duke, and Dobbins [20] studied the intelligent use of wing stiffness tailoring, control surface topological design and active control. The objective was the reduction of the wing induced drag and control improvement of a flexible aircraft.

The main reason for the widespread use of flaps for aeroelastic control during the 80's and 90's was the availability of high authority leading and trailing edge control surfaces on existing wings. Also, discrete control surfaces are perceived to be very efficient for loads control. Supporting that in a parallel field (vibration reduction in helicopter blades), Millot and Friedmann [21] showed that actively controlled flap (ACF) consumes 10-20 times less power than conventional blade control in which the whole blade is rotated at its root by the pitch input. However, it is also known that the associated disadvantage of flaps is the increase in induced drag due to flow separation at the discontinuity between the wing and flap.

Another disadvantage of using flaps is the mechanical complexity associated with its actuation mechanism. Traditional hydraulic actuators add weight penalty to the system, and also have hydraulic and aerodynamic lags. An attempt to solve this problem was made in the late 90's by replacing hydraulic actuators with magnetostrictive ones (e.g., Terfenol-D [25]), piezoelectric devices [22] and shape memory alloys [23].

Shape Deformation Methods for Active Aeroelastic Control

Techniques for actively deforming the wing shape and, thus, altering the resultant aerodynamic loads were in evidence in the late 80's. Various active materials were utilized for this purpose. Among them, piezoelectric materials were the most popular because their bandwidth cover most of the important aeroelastic modes. Shape memory alloys, on contrary, are limited to low frequency applications. They have been utilized in realizing hingeless control surfaces in the Smart Wing program [24]. Shape memory alloys are beyond the scope of this work.

Piezoelectric materials can be used as strain actuators in various forms, and based on their actuation properties they can be widely classified as isotropic and anisotropic actuators.

Isotropic Piezoelectric Actuators

In 1990, Weisshaar and Ehlers [26] applied embedded isotropic piezoelectric material to modify the static aeroelastic behavior of a lifting surface. The wing was modeled as a laminated sandwich structure with piezoelectric layers in the upper and lower skins and active control techniques were used to modify the aeroelastic divergence speed of the wing. Later in 1993, under the Piezoelectric Aeroelastic Response Tailoring Investigation (PARTI), Crawley, Lazarus, and Lin [19, 27, 28] studied aeroelastic control using control surfaces and strain actuation techniques. They used MIMO control method for gust alleviation and flutter suppression on a cantilevered strain actuated wing test article. Piezoelectric actuators were also used in the 90s, among other things, for supersonic panel flutter control by Haleja and Glowasky [29]. Manser, Simpson, et al. [30] used piezoelectric patch actuators for active vertical tail buffet alleviation under the DaimlerChrysler Advanced Aircraft Structures program.

In spite of its widespread usage, authority of isotropic piezoelectric wafers for influencing torsion modes of wings in flutter studies was shown to be limited, and its lack of actuation directionality requires coupling between the actuator and the structural elasticity of the substrate.

Anisotropic Piezoelectric Actuators

Anisotropic strain actuators provide a new degree of design flexibility when dealing with active structures. The ability to tailor the actuation orientation independently of the passive elastic behavior of the structure is highly desirable from an aeroservoelastic point of view.

The first scalable embodiment of anisotropic strain actuator was achieved in the mid-90s through the active

fiber composite (AFC). They have been mostly studied for vibration alleviation in helicopter blades [31, 32, 33] and active aeroelastic tailoring of HALE wings [34]. Another embodiment of anisotropic strain actuator is the macro fiber composite (MFC) [35]. These actuators are currently being studied as a potential means for reducing buffeting loads on twin-tail fighter aircraft flying at high angles-of-attack in a NASA-Langley 1/6th scale active vertical tail model.

Although AFCs and potentially MFCs are being used for different aeroelastic applications, an actuator with a greater level of actuation and potentially better tailored properties is required for high authority applications such as shape control of wing or maneuver enhancement of aircraft. Initial developmental studies indicate that single crystal fiber composite (SCFC) [40] has a very high actuation level compared to that of the presently available AFC. This is because the SCFC fiber is developed from a single crystal that can be grown by different techniques [36]. Figure 2 shows a quantitative comparison of actuation capabilities of two different forms of piezoelectric actuators, i.e., polycrystalline (AFC) and single crystal (SCFC).

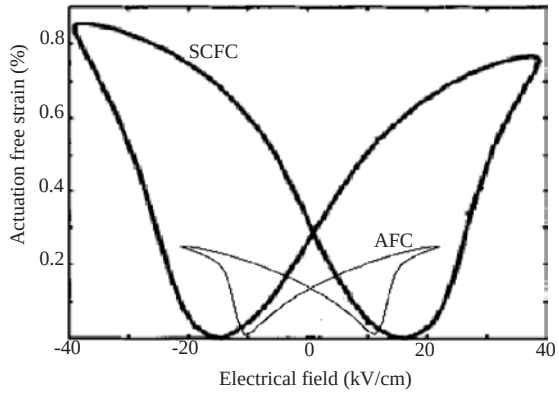

Figure 2: Butterfly curve of a SCFC (tetragonal phase ferroelectric crystal) versus AFC. The butterfly curve of SCFC has been taken from Ref.[40] and the one for AFC from Ref.[41]. Both have undergone advancement in terms of actuation capability ever since.

Three observations may be drawn from the comparison of the two material systems. First, the actuation level that can be achieved by SCFCs is significantly higher than that of the present AFCs. This high level of actuation can potentially be utilized in high authority applications such as maneuver control of Uninhabited Combat Aerial Vehicles (UCAVs). The absence of pilots in UCAVs will allow for experimenting beyond the traditional design limits, which in turn can utilize the higher authority of SCFCs. Secondly, since it is a material under development, the properties of the SCFC can potentially be tailored to meet specific requirements by changing the fiber-matrix ratio, fiber composition, pitch of electrodes, etc. Finally, the behavior of SCFC, as shown in Figure 2, is expected to be nonlinear in the operating range of applied electrical field. This needs nonlinear optimization and control techniques in applications such as maneuver control of UCAVs.

Roll Maneuver Control of UCAVs

One potential application of the high authority SCFCs is in the field of roll maneuver control of UCAVs.

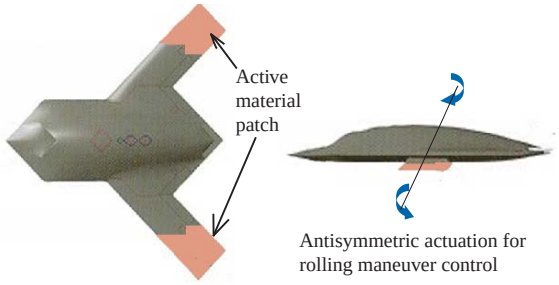

Figure 3: Antisymmetric actuation to achieve rolling maneuver control in UCAV.

As shown in Figure 3, SCFCs can potentially be embedded in the skins of both the wing surfaces, covering the wing either wholly or partially, and rolling motion can be controlled by antisymmetrically actuating the active wings. This is expected to be a step towards realizing a high-performance highly conformable Active Aeroelastic Wing (AAW) configuration for a UCAV, without any complex control surfaces and their internal actuation mechanisms.

OBJECTIVES OF THIS STUDY

The multidisciplinary nature of AAW concept in the active UCAV wing design requires a tight integration of unsteady aerodynamics, structural dynamics, and controls in the presence of distributed embedded actuators and sensors. The modeling of SCFC and its nonlinear mechanisms of actuation along with the aeroservoelastic characteristics of the flexible wing are essential for the success of the concept. To implement the concept, two objectives need to be met:

- Develop a numerical design framework to allow the AAW concept for the active UCAV wing design to be implemented.
- Use the numerical design environment to determine the specifications of the SCFC based actuators required to achieve predetermined targets for roll maneuver. The specifications include the actuator mechanical and active properties, the actuator location inside the wing skin and along the span of the wing, and the actuator ply angles. All of these should be conducted under constraints that arise from limitations due to material failure, wing natural frequencies, and flutter and divergence considerations.

PRELIMINARY STUDY

A preliminary study was done to estimate the roll rates that can be achieved using currently existing AFCs in a generic combat aircraft. Changes in the roll rate level with different AFC layup angles was also studied. The chosen model for this study is based on the generic combat aircraft developed at the Wright Laboratory (WPAFB) [37]. This model has been originally used for roll maneuver control studies using pointwise linear actuator elements in ASTROS [38]. In the present study, the model was imported into MSC/NASTRAN [39] and modified to replace the linear actuators by AFCs.

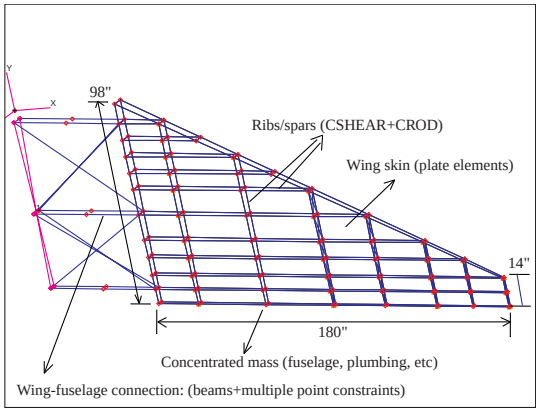

Figure 4: Finite element model of the WPAFB fighter wing in MSC/NASTRAN.

Details of the baseline WPAFB Model

The underlying wing structure, as shown in Figure 4, consists of 10 spars and 6 ribs and was modeled using 167 nodes. Top and bottom skins were modeled with CQUAD4 and CTRIA3 elements (towards the leading edge). Spar and web caps were modeled with CSHEAR and CROD elements. Appropriate single and multi-point constraints were specified for proper simulation of the wing structure connection to the fuselage. An 8000 lbs mass was used to simulate the weight of the fuselage. In addition, different amounts of non-structural mass (totaling 1600 lbs) were distributed amongst different node points on the wing to simulate fuel, plumbing, wiring and fastener weights [37].

The graphite-epoxy composite laminates in the skin were assumed to have $[90, 0, -45, 45]_{sym}$ layup, with 0^0 orientation being parallel to the span of the wing. The thickness of each layer was taken from Ref. [37]. The material properties used in this study are given in the Appendix. A normal mode analysis (SOL 103) was conducted on the finite element model and the natural frequencies were compared to that obtained from Ref. [37]. An exact match confirmed the proper model export from ASTROS to MSC/NASTRAN.

The aerodynamic model uses doublet lattice subsonic method available in MSC/NASTRAN. The aerodynamic grid was constructed in the plane equidistant from the upper and lower structural surfaces. The number of panels was determined by numerical convergence. IPS interpolation scheme [42] was used for data transfer between the aerodynamic grid and the upper surface of the structural grid. This method, although not very accurate for general applications [43], was found to provide similar results as the other two schemes (FPS and TPS) available in MSC/NASTRAN. This is primarily due to the nature of the grids that are almost planar.

Roll Rate Analysis of the WPAFB-AFC Model

Rolling can be achieved by actuating the AFC patches, embedded in the skin, in two ways: (a) shear (ϵ_{12}) deformation, and (b) camber deformation. The wing can be deformed along the camber direction by introducing 90^0 AFC fibers in the upper and lower skins, and then actuating them out-of-phase. The following configurations were used for AFC ply angles for shear deformation:

- $[45_{AFC}/90/0/-45/45/45/-45/0/90/-45_{AFC}]$,
- $[45_{AFC}/90/-45_{AFC}/0/-45/45/45/-45/0/90]$,
- $[90/0/-45/45_{AFC}/45/45/-45/0/90/45_{AFC}]$, and
- Upper skin:
  $[(45_{AFC})_2/90/0/-45/45/45/-45/0/\ 90]$
  Lower skin:
  $[90/0/-45/45/45/-45/0/90/\ (-45_{AFC})_2]$.

where the subscript *'AFC'* refers to the active layers while the other angles refer to the passive substrate of the wing.

The AFCs were distributed all over the wing skin, from the wing tip up to about 30% of the half-span from the aircraft longitudinal axis, since the AFC patches near the thick wing root would not contribute significantly to the wing twist. Also, one or two plies of graphite-epoxy was removed from the baseline layup for each of one or two plies of AFC added to maintain the skin thickness. This gives a total of 24 cases each for the shear and camber actuation options, thus providing a significantly large domain space for studying the sensitivity of roll rate for different AFC configurations. The wing was actuated at $\pm$1000V, and the flight conditions used were Mach number 0.85 and dynamic pressure 7.4 psi (the latter two conditions are from Ref. [37]). The results are plotted in Figure 5.

Conclusions of the Preliminary Study on Roll Maneuver of WPAFB-AFC Wing

Five things stand out from Figure 5. One is that camber actuation is significantly less effective in roll rate control than shear. This is expected because of the wing stiffening due to presence of ribs. Secondly, there is a significant variation (maximum of 30%) in roll rate with change in AFC configuration within each method of actuation. Thirdly, the spikes in case of shear actuation correspond to the configuration with $+45^0_{AFC}$ plies

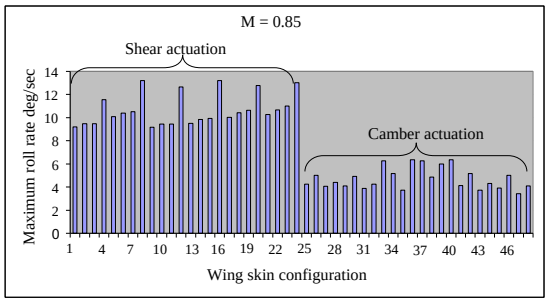

Figure 5: Maximum roll rate of the WPAFB-AFC wing, after being actuated at 1000V, Mach number 0.85 and dynamic pressure 7.4 psi.

on the top of the upper wing skin and -45^0_{AFC} plies on the bottom of the lower wing skin. This is expected for a wing with quasi-isotropic baseline passive layup. Fourthly, by doubling the number of active plies on each skin increases the roll rate by about 10%. Finally, the maximum roll rate level achieved here is 13 deg/sec. Although the passive baseline layup was not properly optimized for the AAW concept, this preliminary study seems to indicate that a more powerful actuator may be needed to achieve the high roll rate levels for low aspect ratio combat aircraft.

ARCHITECTURE OF THE NUMERICAL DESIGN ENVIRONMENT FOR UCAV ROLL MANEUVER STUDY

After the preliminary AFC roll rate study, a broader numerical framework for the UCAV roll maneuver study is developed. Within this framework, various material configurations can be tested on an active UCAV wing for optimum performance.

The framework consists of an optimization loop as shown in Figure 6. In the future, a control module will be added to increase the aeroelastic safety margin for more flexible designs.

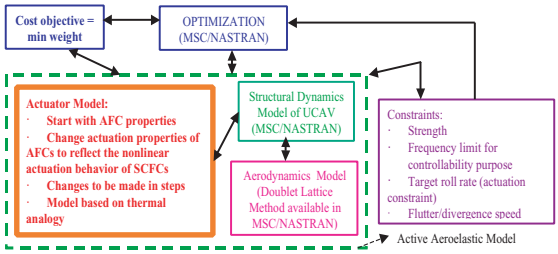

Figure 6: Optimization loop to determine various feasible material configurations for the UCAV.

There are several components associated with this loop, as enumerated below.
(a) Structural Dynamics Model: This is the UCAV finite element model.
(b) Aerodynamics Model: As before, Doublet Lattice Subsonic Method available from MSC/NASTRAN is utilized for the aerodynamics.
(c) Anisotropic Actuator Model: The properties of the anisotropic actuator used in the start of the optimization loop is that of AFC, and the actuation properties are changed in steps with the progress in optimization. The actuators are modeled in MSC/NASTRAN by taking advantage of anisotropic thermal analysis and the following analogy with piezoelectric effects:

$$d_{ij} * V/t = \alpha_{ij} * \Delta T \qquad (1)$$

where i,j refer to a particular material direction, d is the piezoelectric constant, V/t is the electric field applied to the actuators, α is the equivalent coefficient of thermal expansion, and ΔT is the equivalent temperature.
(d) Constraints Implementation: The various constraints in the optimization loop are as follows.

(i) Strength: Tsai-Wu criterion for composite material is used for predicting the failure indices of the UCAV wing for a certain loading condition.

(ii) Frequency limit: A lower limit is imposed on the first symmetric bending frequency of the aircraft, for controllability purpose.

(iii) Roll rate: This is directly associated with the actuation authority.

(iv) Flutter/divergence speed: This makes sure that the configurations are safe from flutter and divergence point of view.

For this study, the values for the loading conditions are taken from the Wright Laboratory study of the fighter wing [37].

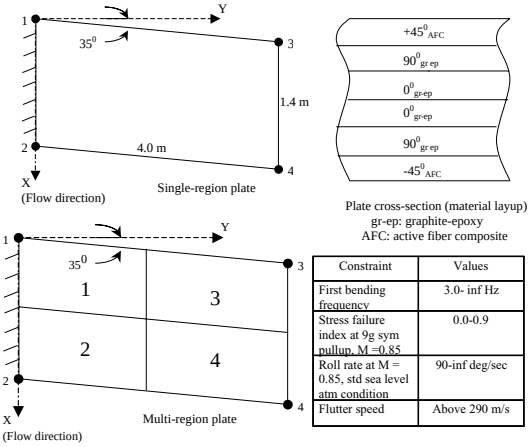

Figure 7: Simple example used for implementing the numerical design environment.

PRELIMINARY TEST OF THE NUMERICAL DESIGN ENVIRONMENT

A cantilevered sweptback plate of dimensions shown in Figure 7 was used as a test example to better understand the numerical design environment. The plate, fixed at side 1-2, was discretized into 8 elements along the X-axis and 12 elements along the Y-axis. For the aerodynamic load cases, the flow was considered to be along the X-axis. 20 panels along the chord and 30 along half-span were taken. The number of elements for

the structural and aerodynamic grids were determined by a separate numerical convergence study.

Two kinds of optimization analyses were performed. In the first case, the thickness of each ply was kept uniform throughout the plate. The following thickness variables were used for optimization: (a) TPLY90, the thickness of the 90^0 graphite-epoxy plies, (b) TPLY0, the thickness of the 0^0 graphite-epoxy plies, and (c) TPLY45, the thickness of the 45^0 active plies. In the second case, the plate was divided into four regions, as shown in the same figure, and the thickness of each ply within a region was kept uniform. The following thickness variables were used for optimization: TPLY90(1-4), TPLY0(1-4), and TPLY45(1-4) where the numbers in parentheses refer to the region.

In both cases, the piezoelectric constant property d_{11} of the active material constituting the top and bottom plies was also taken as an optimization variable and suitable limits imposed to simulate the actuation behavior of SCFC. From the representative butterfly curve of Figure 2, d_{11} was calculated for various voltage levels. The resulting variation of d_{11} with applied voltage to the SCFC is shown in Figure 8. The equivalent α_{11} was calculated from Equation 1, with applied voltage fixed at 1000 V. The mechanical and other properties of SCFC were kept the same as those of AFC.

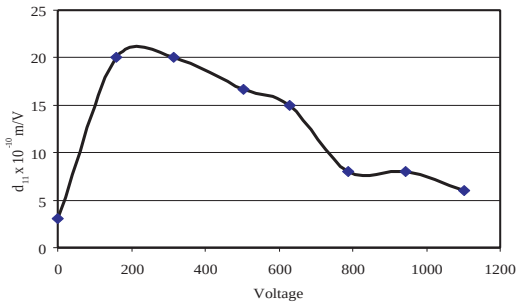

Figure 8: SCFC representative variation of d_{11} with applied voltage.

A modified feasible direction optimization method was used in MSC/NASTRAN and the objective was to minimize the plate mass.

The optimization variables were constrained between upper and lower bounds as follows: all TPLY's were constrained between 0.001 and 0.1 m, while the equivalent α_{11} was constrained between 98.1 and 634.9, representing the possible range of SCFC free strain actuation (as obtained from Figure 8).

The optimization study was conducted in the following way. First each of the performance constraints was implemented individually. Three starting points were used: one at the upper bound of the design variables, the second at the lower bound, and the last one at midpoint between the two bounds. The optimizer was allowed to run till convergence was reached or to a maximum of 40 runs. When the optimization run terminated in the infeasible region, the feasible solution with the least mass was taken.

The next step was to introduce all the constraints simultaneously and perform optimization. In this case, when the optimization using the aforementioned starting points did not lead to a satisfactory global optimum, the solution of the individual constraint run that gives the maximum mass was taken as the starting point for multi-constraint optimization. This solution would be closer to the multi-constraint optimum one when compared to the solution of the individual constraint run that gives the minimum mass. Also, an additional optimization was done by fixing α_{11} at its maximum level (i.e., 634.9) to simulate the maximum authority actuator (for a fixed d_{11}/d_{12} ratio and given stiffness). Tables 1 and 2 show some of the results.

Table 1: Constraint values in the optimization of the single region plate. Units: mass in kg, frequency in Hz, roll in deg/sec, and α_{11} in 10^{-8} units. Notations: fp_{max} = maximum failure index of any ply, d_{290} = flutter damping factor at 290 m/s, and α_{11} = equivalent coefficient of thermal expansion of active material.

Constraints	Mass	Final constraint value
Frequency constraint	281.6	Freq = 3.0
Stress constraint	512.8	fp_{max} = 0.7228
Roll constraint	93.4	Roll = 195.9, α_{11} = 192.8
Flutter constraint	65.6	d_{290} = -12.500
All constraints	1000.4	Freq = 3.4, fp_{max} = 0.2155, Roll = 826.2, α_{11} = 634.9, d_{290} = -2.619

Table 2: Constraint values in the optimization of the multi-region plate. Units and notations same as in Table 1.

Constraints	Mass	Final constraint value
Frequency constraint	145.6	Freq = 3.0
Stress constraint	501.4	fp_{max} = 0.9907
Roll constraint	93.6	Roll = 195.9, α_{11} = 192.8
Flutter constraint	65.6	d_{290} = -12.500
All constraints	1115.6	Freq = 3.0, fp_{max} = 0.0338, Roll = 252.5, α_{11} = 98.1, d_{290} = -2.142
All constraints with max actuation	4148.2	Freq = 11.0, fp_{max} = 0.0001, Roll = 414.4, α_{11} = 634.9, d_{290} = -0.5574

As expected, increasing the number of design variables results in lower mass solutions. This is due to the greater design flexibility, allowing the solution to find better points in the design space. However, the results of "roll" and "flutter," and in a certain sense "stress," did not significantly change from Table 1 to 2. Also, the result from "all constraints" in Table 2 has a higher mass than the corresponding one in Table 1. This is because the optimization step size chosen for the former case was not refined enough. By reducing the step size where searches are conducted, the solutions presented here can actually be improved. Finally, it may be remarked that when α_{11} was fixed at its highest value, the

optimizer converged to a greater-mass solution with a much higher roll rate response due to the higher authority of the actuator. This also serves to illustrate that decreasing the number of design variables results in solutions with greater mass.

The simple example presented above served to show that the proposed framework should be able to handle a more realistic model with all the constraints involved in the problem.

OPTIMIZATION OF A UCAV-LIKE WING

Having ascertained the viability of the aforementioned framework, the final step was to implement the optimization loop for a UCAV-like model. The model was created based on the publicly available data of the Boeing X-45A [44]. Information was also taken from data available for similar aircraft.

Details of the UCAV model

The underlying half-UCAV structure, as shown in Figure 9, consists of an aluminum fuselage frame covered with skin and extending up to the wings. It was idealized using 324 nodes. The upper and lower skins and the aluminum frame were idealized with CQUAD4 elements. Appropriate multi-point constraints were specified at the longitudinal axis of the aircraft for proper simulation of different boundary conditions of the aircraft. In addition, different amounts of non-structural mass (totaling 5039 kg for the full aircraft) were distributed amongst different node points on the aircraft to simulate fuel, plumbing, wiring and fastener weights, engine, landing gears, and weapons.

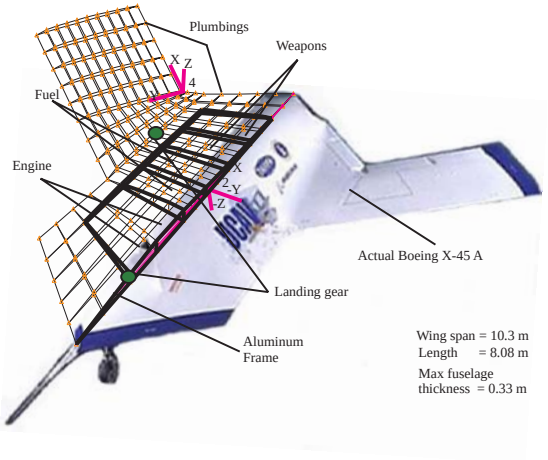

Figure 9: Finite element discretization of the UCAV together with the original X-45A. Generic data was used in the finite element model due to public unavailability of complete specifications. The X-axis of the reference frame "4" gives the 0^0 ply direction for the wing and wing-fuselage intersection surfaces, while that of reference frame "2" gives the direction for fuselage surfaces.

The skin in the fuselage section consists of a quasi-isotropic graphite-epoxy layup: $[90/0/-45/45]_{sym}$. Active fibers, denoted here by the subscript *'A'*, were embedded in the wing upper and lower skins to obtain the following layups: $[+45_A]_2/[90/0/-45/45]_{sym}$ and $[90/0/-45/45]_{sym}/[-45_A]_2$.

A specially-developed MATLAB [45] code was created to generate the structural finite element mesh for the MSC/NASTRAN input files. The model has the flexibility of changing the number of nodes, the airfoil used for the wings, and the cross-section of the fuselage. A 5% thick NPLX transonic airfoil [46] was used for this study. As in the case of the WPAFB wing, the aerodynamic model of the UCAV uses doublet lattice subsonic method. The grid was constructed at the base plane of the aircraft and IPS was used for data transfer between the upper aircraft surface and the aerodynamic grid.

Details of the optimization process

As in the case of the simple plate optimization, the thickness of each of the 90^0, 0^0 and $\pm 45^0$ plies as well as the equivalent α_{11} of the SCFC were taken as design variables. The bounds for the thickness variables were (0.000125, 0.1) m for graphite-epoxy and (0.000315, 0.1) m for SCFC, while that for α_{11} were between 98.1 and 634.9. Here, the lower thickness bounds correspond to 1 ply of the corresponding material.

For this study, the half-aircraft model was divided into four regions, as shown in Figure 10. The division was done for both top and bottom surfaces of the aircraft. Regions 1 and 2 were further subdivided into two subregions, as shown in Figure 10.

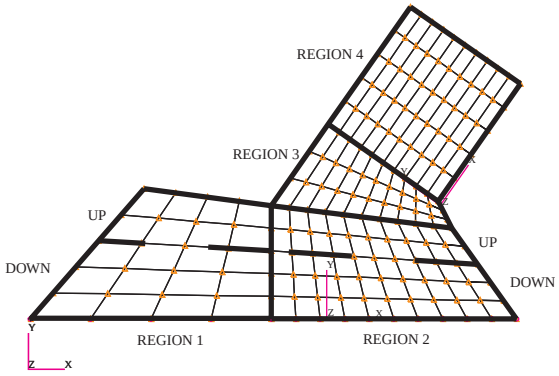

Figure 10: UCAV model divided into different regions for optimization studies.

The thickness values of material plies are uniform within each region. The thickness of the aluminum frame was kept fixed at 0.005 m. The SCFC plies were introduced only in region 4 and the upper and lower wing surfaces were considered independent during optimization.

The performance constraints with respect to frequency, stress, roll and flutter were kept the same as that in the simple plate problem. Also, optimization was started from three points: lower and upper bounds, and midpoint of the domain. Each of the constraints was introduced separately, and corresponding minimum weight design found. Then all the constraints were in-

troduced simultaneously and the analysis was repeated. The optimization was done in a Dell Precision 410 workstation with 256 MB RAM.

It was observed that the optimizer did one of two things for the individual constraint case: (1) it did not move from the starting point, or (2) it converged to the lower bounds of the design variables. When all the constraints were introduced, the optimizer showed one of the following results: (1) it did not move from the starting point, as before, or (2) it stopped with an error due to lack of memory.

To reduce the problem size, α_{11} was fixed at the upper bound of 634.9. Also, instead of explicitly checking for failure of all finite elements of the aircraft in the optimizer, only the most critical stress areas were checked during an optimization loop. By numerical investigation, the most critical areas were found to be REGION 1 UP and REGION 4 in Figure 10. The failure indices of other regions of the aircraft were checked manually after optimization. Also the ply variables corresponding to REGIONs 1 and 2 DOWN were treated as fixed parameters for the optimization problem. Again by numerical investigation, these thickness variables were each set to be 0.0025 m (20 plies) while the starting point for all other graphite-epoxy variables was kept at 0.0005 m (4 plies) and that of the active plies was 0.001575 m (5 plies). Optimization was conducted and the minimum weight design satisfying all constraints as closely as possible was determined.

Results of Optimization

Table 3 presents the results of the optimization. The maximum failure index of 0.9210 is within acceptable range. The frequency is above the 3.0 Hz limit. The roll rate is 92.7 deg/sec, above the specified target. Finally, the damping factor at 290 m/s is slightly negative which implies that the aircraft is flutter-free below 290 m/s at M = 0.85, although with a small margin.

Table 3: Constraint values in the optimization of the UCAV. Units and notations same as in Table 1. Mass refers to the half-aircraft model.

Particulars	Mass	Constraint value
All constraints	3945	Freq = 5.3, fp_{max} = 0.9210, Roll = 92.7, α_{11} = 634.9, d_{290} = -1.6952x10^{-2}

The thickness distribution of all the plies are given in the Figures 11-14. It can be seen that the thickness of all graphite-epoxy plies is maximum near the longitudinal axis of the aircraft due to strength consideration. The figure also shows the asymmetry of thickness of all the plies about the lateral plane of the aircraft (that divides the top and bottom surfaces). The distribution of the different plies in the aircraft is governed by a host of factors, including wing sweepback angle of 65^0, strength requirement due to pullup, roll rate requirement above 90 deg/sec, flutter and natural frequency mode shapes

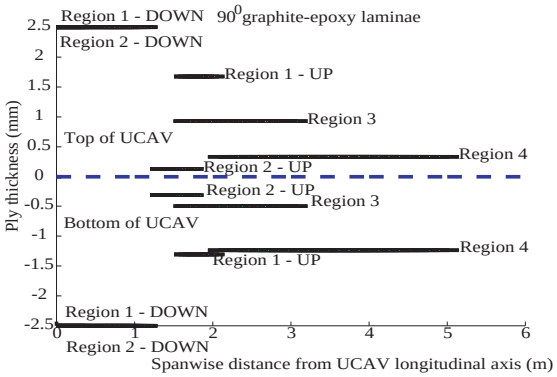

Figure 11: Laminae thickness profile of the 90^0 graphite-epoxy region of the UCAV after optimization.

that satisfy the respective flutter speed and frequency limits. It may be noted that the thickness values shown here need to be converted to the closest number representing integer number of plies, and that this solution need to be checked for feasibility. The UCAV design study may be further refined by using different material layups, airfoils, and fuselage shapes.

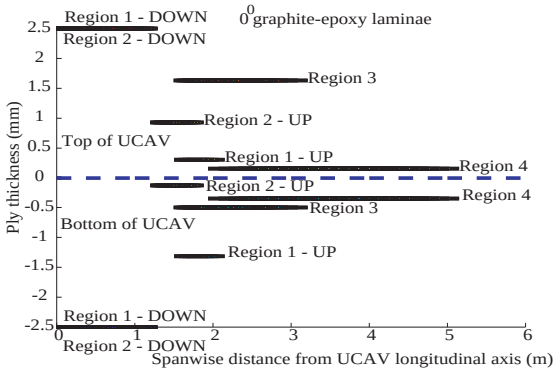

Figure 12: Laminae thickness profile of the 0^0 graphite-epoxy region of the UCAV after optimization.

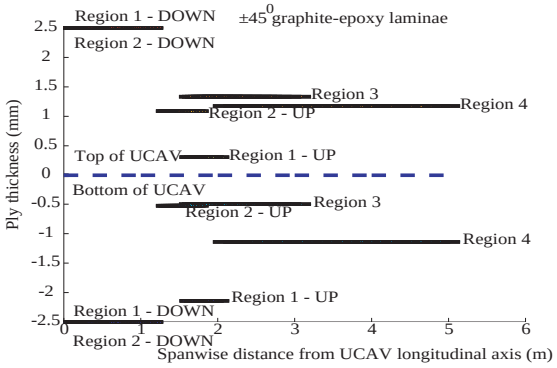

Figure 13: Laminae thickness profile of the $\pm 45^0$ graphite-epoxy region of the UCAV after optimization.

CONCLUDING REMARKS

Design of modern high-speed combat aircraft could take advantage of active aeroelastic tailoring to aug-

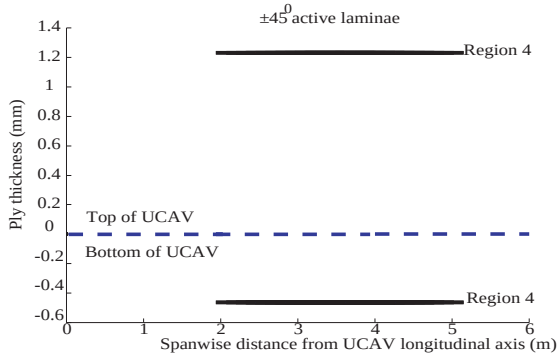

Figure 14: Laminae thickness profile of the $\pm 45^0$ active region of the UCAV after optimization.

ment its performance. With the advent of high authority anisotropic actuators, wing warping can potentially be used in the next generation of UCAV to achieve roll controllability instead of traditional discrete control surfaces. To study this problem, a suitable numerical design environment was developed to include the novel aspects of integrally distributed anisotropic piezocomposite actuators in a composite wing construction. Using this framework, roll maneuver control through wing warping can be determined. The numerical framework was tested for relatively simple models and performed according to specifications. A Boeing X-45A-based UCAV model was used to assess the authority requirement on the piezocomposite actuators for achieving a representative roll rate while satisfying other design constraints. The results showed that current state-of-the-art technology on anisotropic piezocomposite actuators (e.g., active fiber composites) do not have the authority needed for wing warping control. A three to four-fold increase in actuation authority is needed to enable this control approach for this type of aircraft. The expected properties of the single-crystal fiber composites currently under development would provide the desirable authority. Results showed that the X-45A-like aircraft can achieve over 90°/s roll rate with no more than 1.3-mm thick active regions on each surface of the wing. The results presented in this paper explored only part of the possible design space. In future, studies need to be conducted on different ply layups, airfoils, fuselage cross sections, and non-structural mass distribution. Also, higher number of design variables should be considered to obtain lower mass solutions. More automation is also desirable for the optimization process, eliminating significant human intervention needed on the current implementation. The small flutter margin obtained from the optimization runs shows that it will be an active constraint is such concept. A control module should be added to the numerical framework to allow the study of stability augmentation using the already present actuators on the system. Finally, aerodynamic modeling issues and sensor architecture should be addressed in future studies of distributed anisotropic piezocomposite actuators for UCAV applications.

ACKNOWLEDGEMENTS

The authors gratefully acknowledge the technical interactions with Dr. Roy Ikegami (Boeing Phantom Works) and Dr. Narendra Khot (AFRL/VA) during the course of this study. This work was sponsored by AFOSR-DARPA's Single Crystal Program through Boeing contract No. KD5947. The Government Program Managers are Dr. Spencer Wu and Dr. Wallace Smith.

APPENDIX

The properties of various materials used in this study have been enlisted below.

1. Mechanical properties of aluminum:
   (a) $E = 3.0\text{x}10^7$ psi ($70\text{x}10^9$ Pa)
   (b) $G = 1.127\text{x}10^7$ psi ($26.315\text{x}10^9$ Pa)
   (c) $\nu = 0.33$
   (d) $\rho = 2.591\text{x}10^{-4}$ slug/in^3 (2700 kg/m^3)
   (e) Yield stress = $3.1183\text{x}10^4$ psi ($215\text{x}10^6$ Pa)
2. Mechanical properties of graphite-epoxy:
   (a) Ply thickness = 0.125 mm
   (b) $E_1 = 2.62\text{x}10^7$ psi ($1.43\text{x}10^{11}$ Pa)
   (c) $E_2 = 1.49\text{x}10^6$ psi ($9.81\text{x}10^9$ Pa)
   (d) $\nu_{12} = 0.28$ (0.3)
   (e) $G_{12} = 1.04\text{x}10^6$ psi ($6\text{x}10^9$ Pa)
   (f) $\rho = 1.5\text{x}10^{-4}$ slug/in^3 (1545 kg/m^3)
   (g) Interlaminar shear strength = 1800 psi ($1.185\text{x}10^7$ Pa)
   (h) $X_t = 218000.$ psi ($2.356\text{x}10^9$ Pa)
   (i) $X_c = 218000.$ psi ($2.356\text{x}10^9$ Pa)
   (j) $Y_t = 5800.$ psi ($5\text{x}10^7$ Pa)
   (k) $Y_c = 5800.$ psi ($5\text{x}10^7$ Pa)
   (l) $S = 35700.$ psi ($1.05\text{x}10^8$ Pa)
3. Mechanical properties of orthotropic AFC:
   (a) Ply thickness = 0.315 mm
   (b) $d_{11} = 309$ pm/V
   (c) $d_{12} = -129$ pm/V
   (d) $E_1 = 4.377\text{x}10^6$ psi ($3.018\text{x}10^{10}$ Pa)
   (e) $E_2 = 2.163\text{x}10^6$ psi ($1.491\text{x}10^{10}$ Pa)
   (f) $\nu_{12} = .454$ (.454)
   (g) $G_{12} = 0.744\text{x}10^6$ ($5.13\text{x}10^9$ Pa)
   (h) $\rho = 4.559\text{x}10^{-3}$ slug/in^3 (4060 kg/m^3)
   (i) Interlaminar shear strength = 1800 psi ($1.185\text{x}10^7$ Pa)
   (j) $X_t = 80974.5$ psi ($5.583\text{x}10^8$ Pa)

(k) X_c = 80974.5 psi (5.583x10^8 Pa)

(l) Y_t = 11896.5 psi (8.203x10^7 Pa)

(m) Y_c = 11896.5 psi (8.203x10^7 Pa)

(n) S = 9282.4 psi (6.4x10^7 Pa)

The SCFC properties were kept the same as those of AFC, except for d_{11} which was used as a design variable.

REFERENCES

[1] M. H. Shirk, T. J. Hertz, and T. A. Weisshaar. Aeroelastic Tailoring - Theory, Practice, and Promise. *Journal of Aircraft*, Vol. 23, No. 1, Jan. 1986, pp. 6-18.

[2] M. M. Munk. Propeller Containing Diagonally Disposed Fibrous Material. U.S. Patent 24843081111, Oct. 1949.

[3] M. E. Waddoups. *Private communication.* General Dynamics, Ft. Woth Div., Ft. Worth, Texas, July 1983.

[4] L. A. McCullers, and R. W. Lynch. Dynamic Characteristics of Advanced Filamentary Composite Structures, Volume 2 - Aeroelastic Synthesis Procedure Development. AFFDL-TR-73-111, Sept. 1974.

[5] M. A. Price. Structural Development Design Methodology. NASA CR-144886, Oct. 1979.

[6] N. J. Krone, Jr. Forward Swept Wing Flight Demonstrator. AIAA Paper 80-1882, Aug. 1980.

[7] J. M. Housner, and M. Stein. Flutter Analysis of Swept Wing Subsonic Aircraft with Parameter Studies of Composite Wings. NASA TN-D7539, Sept. 1974.

[8] T. A. Weisshaar. Aeroelastic Tailoring of Forward Swept Composite Wings. *Journal of Aircraft*, Vol. 18, Aug. 1981, pp. 669-676.

[9] S. J. Hollowell, and J. Dugundji. Aeroelastic Flutter and Divergence of Stiffness coupled, Graphite-Epoxy Cantilevered Plates. *Presented at the 23rd AIAA/ASME/ASCE/AHS Structures, Structural Dynamics and Materials Conference*, AIAA Paper 82-0722, May 1982.

[10] D. Gimmestad. An Aeroelastic Optimization Procedure for Composite High Aspect Ratio Wings. AIAA 79-0726, 1979.

[11] S. D. Gratke, and J. G. Williams. Analysis/Theory of Controlled Configured Structures (CCS). AIAA Paper 77-1212, Aug. 1977.

[12] C. E. S. Cesnik, D. H. Hodges, and M. J. Patil. Aeroelastic Analysis of Composite Wings. AIAA-96-1444-CP, 1996.

[13] L. Librescu, and S. Thangjitham. Analytical Studies on Static Aeroelastic Behavior of Forward Swept Composite Wing Structure. *Journal of Aircraft*, Vol. 28, No. 2, Feb. 1991, pp. 151-157.

[14] L. Librescu, and O. Song. On the Static Aeroelastic Tailoring of Composite AircraftSwept Wings Modeled as thin-Walled Beam Structures. *Composites Engineering*, Vol. 2, No. 5-7, 1992, pp. 497-512.

[15] T. A. Weisshaar, C. Nam, and A. Bastista-Rodriguez. Aeroelastic Tailoring for Improved UAV Performance. *39th AIAA/ASME/ASCE/AHS/ASC Structures, Structural Dynamics and Materials Conference, Long beach, California*, April 1998.

[16] M. C. Sandford, I. Abel, and D. L. Gray. Development and Demonstration of a Flutter-Suppression System using Active Controls. NASA-TR-R-450, December 1975.

[17] C. Hwang, B. Winther, G. Mill, T. Noll, and M. Farmer. Demonstration of Aircraft Wing/Store Flutter Suppression Systems. *Journal of Aircraft*, Vol. 16, No. 8, 1979, pp. 557-563.

[18] B. Perry III, V. Mukhopadhayay, S. T. Hoadley, et al. Digital-Flutter-Suppression-System Investigations for the Active Flexible Wing Wind-Tunnel Model. AIAA-90-1074-CP, pp. 1571-1581.

[19] K. B. Lazarus, E. F. Crawley, and C. Y. Lin. Fundamental Mechanisms of Aeroelastic Control with Control Surface and Strain Actuation. AIAA-91-0985-CP, 1991, pp. 1817-1831.

[20] T. A. Weisshaar, D. K. Duke, and A. Dobbins. Active Aeroelastic Tailoring with Adaptive Continuous Control Surfaces. AIAA-2000-1619, pp. 1-11.

[21] T. A. Millott, and P. P. Friedmann. Vibration reduction in helicopter rotors using an actively controlled partial span trailing edge flap located on the blade. *Journal of Guidance, Control and Dynamics*, Vol. 18, No. 4, July-August 1995, pp. 664-673.

[22] N. A. Koratkar, and I. Chopra. Testing and validation of a Froude scaled helicopter rotor model with piezo-bimorph actuated trailing edge flaps. *Smart structures and integrated systems; Proceedings of the SPIE Conference, San Diego, California*, Mar. 3-6, 1997.

[23] D. C. Lagoudas, J. K. Strelec, J. Yen, and M. A. Khan. Intelligent design optimization of a shape memory alloy actuated reconfigurable wing. *Society of Photo-Optical Instrumentation Engineers (SPIE Proceedings. Vol. 3984)*, 2000, p. 338-348.

[24] J. N. Kudva, C. A. Martin, L. B. Scherer, et al. Overview of the DARPA/AFRL/NASA

Smart Wing program. *Society of Photo-Optical Instrumentation Engineers, (SPIE Proceedings. Vol. 3674)*, 1999, p. 230-236

[25] V. Giurgiutiu. Recent Advances in Smart-Material Rotor Control Actuation. *41st Structures, Structural Dynamics, and Materials Conference, Atlanta, Georgia*, Apr. 3-6, 2000.

[26] T. A. Weisshaar, and S. M. Ehlers. Static aeroelastic behavior of an adaptive laminated piezoelectric composite wing. AIAA-90-1078-CP, April 1990, pp. 1611-1623.

[27] E. F. Crawley, and C. Lin. Strain Actuated Aeroelastic Control. SERC Report #2-93, Massachusetts Institute of Technology, 1993.

[28] E. F. Crawley, and C. Lin. Towards Optimal strain Actuated Aeroelastic Control. SERC Report #3-96, Massachusetts Institute of Technology, 1996.

[29] P. Haleja, and R. Glowasky. Application of piezoelectric elements in supersonic panel flutter suppression. *AIAA, AHS, and ASEE, Aircraft Design Systems and Operations Meeting, Baltimore, Maryland*, Sept. 23-25, 1991.

[30] R. Manser, J. Simpson, J. Becker, J. Duerr, E. Floeth, U. Herold-Schmidt, H. Stark, and H. W. Zaglauer. Fin-buffet alleviation via distributed piezoelectric actuators-Full scale demonstrator tests. *Industrial and commercial applications of smart structures technologies; Proceedings of the Meeting, Newport Beach, California*, Mar. 2-4, 1999.

[31] W. K. Wilkie, W. K. Belvin, and K. C. Park. Helicopter dynamic stall suppression using piezoelectric active fiber composite rotor blades. *39th AIAA/ASME/ASCE/AHS/ASC Structures, Structural Dynamics, and Materials Conference, Long Beach, California*, Apr. 20-23, 1998.

[32] J. P. Rodgers, and N. W. Hagood. Hover testing of a 1/6th Mach-scale CH-47D blade with integral twist actuation. *9th International Conference on Adaptive Structures and Technologies, Boston, Massachusetts*, Oct. 14-16, 1998.

[33] S. Shin, C. E. S. Cesnik, and M. L. Wilbur. Dynamic response of active twist rotor blades. *AIAA/ASME/ASCE/AHS/ASC Structures, Structural Dynamics, and Materials Conference and Exhibit, 41st, Atlanta, Georgia*, Apr. 3-6, 2000.

[34] C. E. S. Cesnik, M. Ortega-Morales, and M. J. Patil. Active aeroelastic tailoring of high aspect ratio composite wings. *41st AIAA/ASME/ASCE/AHS/ASC Structures, Structural Dynamics, and Materials Conference, Atlanta, Georgia*, Apr. 3-6, 2000.

[35] W. K. Wilkie, R. G. Bryant, et al. Low-Cost Piezocomposite Actuator for Structural Control Applications. *SPIE 7th Annual International Symposium on Smart Structures and Materials, Newport Beach, California*, March 5-9, 2000.

[36] G. W. Farrey, A. N. Soukhojak, S. Sheets, and Y.-M. Chiang. Growth and Characterization of Na1/2Bi1/2TiO3-K1/2Bi1/2TiO3-BaTiO3 Single Crystal Piezoelectrics. *IEEE International Symposium on Applications of Ferroelectrics, 24-27 Aug. 1998, Montreux, Switzerland*, June 1999, pp. 551-554.

[37] N. S. Khot, and J. V. Zweber. Lift Efficient Composite Flexible Wing for Rolling Manuever without Ailerons. AIAA 2000-1333, April 2000.

[38] D. J. Neill, and D. L. Herendeen. *Automated Structural Optimization System (ASTROS) Vol. I Users Manual*. AFWAL TR-93-3025, March 1993.

[39] K. Kevin (Ed.). *MSC/NASTRAN - Quick Reference Guide (Version 70.5)*. MacNeal Schwendler Corporation Publication (www.msc.com),1998.

[40] Y.-M. Chiang, G. W. Farrey, and A. N. Soukhojak. Lead-free High-Strain Single-Crystal Piezoelectrics in the Alkaline-Bismuth-Titanate Perovskite Family. *Applied Physics Letters*, Vol 73, Number 25, December 1998.

[41] J. P. Rodgers, and N. W. Hagood. Development of an Integral twist-Actuated Rotor Blade for Individual Blade Control. *AMSL Report #98-6.*

[42] *MSC/Flight Loads and Dynamics Version 1 User's Guide*. MacNeal Schwendler Corporation Publication (www.msc.com), October 1998.

[43] M. J. Smith, C. E. S. Cesnik, D. H. Hodges, and K. J. Moran. An evaluation of computational algorithms to interface between CFD and CSD methodologies. *AIAA/ASME/ASCE/AHS/ASC Structures, Structural Dynamics and Materials Conference and Exhibit, 37th, Salt Lake City, Utah*, Apr. 15-17, 1996.

[44] G. Goebel. *Air Vectors/Aviation Pages: Unmanned Aerial Vehicles, Chapter 13: UCAVs and MAVs.* http://vectorsite.tripod.com/avuavd.html. February 2001.

[45] *MATLAB − The language of technical computing, Release 11 (MATLAB 5.3 Product Family)*. MathWorks Publication (www.mathworks.com), 1999.

[46] M. Selig. *UIUC Airfoil Data Site.* http://www.uiuc.edu/ph/www/m−selig/ads/coord_database.html. February 2000.